



Article

The Extraction of Coupling-of-Modes Parameters in a Layered Piezoelectric Substrate and Its Application to a Double-Mode SAW Filter

Lingqi Li ¹, Qiaozhen Zhang ^{1,*}, Yang Yang ¹, Baichuan Li ¹, Yahui Tian ^{2,*}, Xiangyong Zhao ¹ and Sulei Fu ³

¹ The College of Information, Mechanical and Electrical Engineering, Shanghai Normal University, Shanghai 200233, China; 1000446645@smail.shnu.edu.cn (L.L.); yyang@shnu.edu.cn (Y.Y.); 1000494740@smail.shnu.edu.cn (B.L.); xyzhao@shnu.edu.cn (X.Z.)

² State Key Laboratory of Acoustics, Institute of Acoustics, Chinese Academy of Sciences, Beijing 100190, China

³ The Key Laboratory of Advanced Materials (MOE), School of Materials Science and Engineering, Tsinghua University, Beijing 100084, China; fusulei@mail.tsinghua.edu.cn

* Correspondence: zhangqz@shnu.edu.cn (Q.Z.); tianyahui@mail.ioa.ac.cn (Y.T.)

Abstract: This paper presents an advanced method that combines coupling-of-modes (COM) theory and the finite element method (FEM), which enables the quick extraction of COM parameters and the accurate prediction of the electroacoustic and temperature behavior of surface acoustic wave (SAW) devices. For validation, firstly, the proposed method is performed for a normal SAW resonator. Then, the validated method is applied to analysis of an I.H.P. SAW resonator based on a 29°YX–LT/SiO₂/SiC structure. Via optimization, the electromechanical coupling coefficient (K^2) is increased up to 13.92% and a high quality (Q) value of 1265 is obtained; meanwhile, the corresponding temperature coefficient of frequency (TCF) is -10.67 ppm/°C. Furthermore, a double-mode SAW (DMS) filter with low insertion loss and excellent temperature stability is also produced. It is demonstrated that the proposed method is effective even for SAW devices with complex structures, providing a useful tool for the design of SAW devices with improved performance.

Keywords: surface acoustic wave; coupling of modes; layered structure; finite element method



Citation: Li, L.; Zhang, Q.; Yang, Y.; Li, B.; Tian, Y.; Zhao, X.; Fu, S. The Extraction of Coupling-of-Modes Parameters in a Layered Piezoelectric Substrate and Its Application to a Double-Mode SAW Filter. *Micromachines* **2023**, *14*, 2205. <https://doi.org/10.3390/mi14122205>

Academic Editor: Huikai Xie

Received: 10 November 2023

Revised: 28 November 2023

Accepted: 1 December 2023

Published: 3 December 2023



Copyright: © 2023 by the authors. Licensee MDPI, Basel, Switzerland. This article is an open access article distributed under the terms and conditions of the Creative Commons Attribution (CC BY) license (<https://creativecommons.org/licenses/by/4.0/>).

1. Introduction

Surface acoustic wave (SAW) devices have been widely used in wireless communication systems; particularly, filters and duplexers based on SAW resonators are mass-produced and applied in the radio frequency (RF) front-end due to their advantages of high isolation, low insertion loss, etc. With the advent of the 5G era, there is a growing demand for SAW devices in terms of their high frequency, large electromechanical coupling coefficient (K^2), high quality (Q), good temperature coefficient of frequency (TCF) etc.

The performance of SAW devices mainly depends on their piezoelectric substrates. A normal SAW devices on bulk piezoelectric single-crystal materials such as lithium tantalate (LiTaO₃, LT) and lithium niobate (LiNbO₃, LN) have a limitation to their high frequency and Q factor [1–9]. To solve these challenges, T. Takai et al. proposed the I.H.P. SAW device based on a LiTaO₃/SiO₂/AlN/Si multi-layered structure and demonstrated that the resonators employing I.H.P. SAW device offers higher Bode- Q values of over 6000 at 0.9 GHz to 1900 at 3.5 GHz and a very small TCF of -8 ppm/°C [4]. Because of increasingly stringent requirements for performance enhancement, techniques for the analysis and design of SAW devices on such layered piezoelectric substrates with more complex structures are called for [10,11].

In the available numerical simulation techniques, the coupling-of-modes (COM) model is commonly used and proven to be an efficient modeling approach to design SAW devices [10,12–15]. However, the COM model is a phenomenological model, and its COM parameters have to be first determined either via measurements or precise theoretical

numerical methods, for example the finite element method (FEM), or the boundary element method combined with a finite element method (FEM/BEM) [16–21]. Many SAW researchers have made efforts to precisely extract COM parameters. V. Plessky et al. proposed a two-parameter model that approximates the dispersion of leaky waves by characterizing the dispersion relationship of pure surface shear waves propagating in a Bragg grating within the forbidden band [22]. B. P. Abbott and K. Hashimoto et al. further combined the V. Plessky dispersion relation with the COM theory, establishing the STW-COM model and providing a method for extracting STW-COM parameters [23]. The current COM models take into account phenomena including the excitation, propagation, and scattering of surface acoustic waves, and simulate normal SAW devices well. Nevertheless, temperature-dependent COM parameter extraction is still absent.

Therefore, this work proposes a new method combining the COM model with multi-physics quasi-3D periodic FEM model considering the temperature field, which enables the quick and accurate prediction of electroacoustic properties and temperature behavior for both normal and layered SAW devices. For validation, the admittances of two resonators based on 36°YX-LT and $36^\circ\text{YX-LT/SiO}_2/\text{SiC}$ are calculated by using the P -matrix with the extracted COM parameters. Then, the proposed method is employed in the simulation of a full-sized double-mode SAW (DMS) filter, and its temperature behavior is studied and discussed. Furthermore, a design of a high-performance DMS filter with low insertion loss and improved temperature stability is achieved.

2. Experimental Methods

2.1. COM Theory and P -Matrix Model

The materials in Figure 1 depict a basic SAW transducer structure. The COM model is widely employed to investigate the coupling behavior of two counter-propagating acoustic waves in a periodic grating structure.

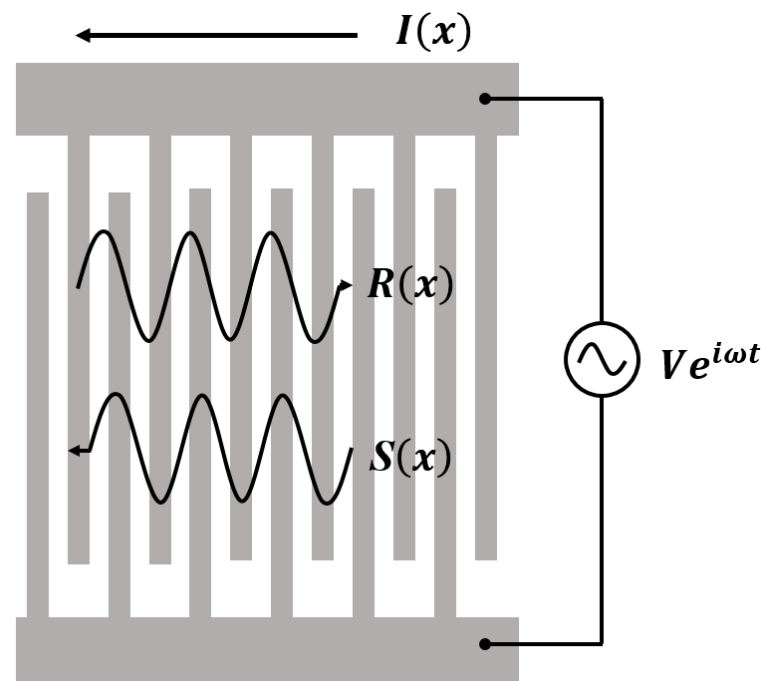


Figure 1. Propagation of SAW in periodic structure.

It is assumed that there exist two counter-propagating acoustic wave modes $R(x)$ and $S(x)$ in an infinitely long periodic grating array. These modes couple to each other through the interdigital reflection effect of the metal grating. Additionally, an external excitation source alternating the voltage, V , on the transducer stimulates acoustic waves, which perturbs the forementioned wave modes. The existence of electrodes on the surface

affects the SAW velocity of the free surface and introduces mode coupling. Assuming linear coupling between amplitude, voltage, and current, the COM equations can be written as follow [10]:

$$\begin{cases} \frac{dR(x)}{dx} = -i\Delta R(x) + i\kappa S(x) + i\alpha V, \\ \frac{dS(x)}{dx} = -i\kappa^* R(x) + i\Delta S(x) - i\alpha^* V, \\ \frac{dI(x)}{dx} = -2i\alpha^* R(x) - 2i\alpha S(x) + i\omega CV, \end{cases} \quad (1)$$

where κ represents the coupling coefficient, α signifies the excitation coefficient, C indicates the static capacitance, and Δ denotes the detuning parameter, which is defined by the following:

$$\Delta = \frac{\omega}{v} - k_0 - j\gamma, \quad (2)$$

where ω is given by $\omega = 2\pi f$, in which f is the frequency of the two waves. v denotes the effective SAW velocity, k_0 indicates propagation wave number, and γ represents attenuation. In Equation (1), the five independent variables including v , κ , α , γ , and C are COM parameters that need to be determined.

Under the linear assumption, the transducer can be equivalently represented by a three-port matrix, which consists of two acoustic ports and one electrical port. Therefore, the solutions to the equations of COM can be obtained using the P -matrix [10]:

$$\begin{bmatrix} b_1 \\ b_2 \\ I \end{bmatrix} = \begin{bmatrix} P_{11} & P_{12} & P_{13} \\ P_{21} & P_{22} & P_{23} \\ P_{31} & P_{32} & P_{33} \end{bmatrix} \begin{bmatrix} a_1 \\ a_2 \\ V \end{bmatrix}. \quad (3)$$

The matrix only considers the physical quantities at its boundaries, including the incident acoustic waves (a_1 and a_2), the outgoing acoustic waves (b_1 and b_2), the input voltage V , and the current I flowing into it. Assuming the COM parameters are known, the P -matrix unit can be calculated using the following equation [10]:

$$\begin{aligned} P_{11} &= \frac{j\kappa^* \sin(LD)}{D\cos(LD) + j\Delta \sin(LD)} \\ P_{12} = P_{21} &= \frac{(-1)^{2N} D}{D\cos(LD) + j\Delta \sin(LD)} \\ P_{22} &= \frac{j\kappa \sin(LD)}{D\cos(LD) + j\Delta \sin(LD)} \\ P_{13} &= -Np \frac{\sin(LD/2)}{LD/2} \frac{(\Delta\alpha^* + \kappa^* \alpha) \sin(LD/2) - j\alpha^* D\cos(LD/2)}{D\cos(LD) + j\Delta \sin(LD)} \\ P_{23} &= -(-1)^{2N} Np \frac{\sin(LD/2)}{LD/2} \frac{(\Delta\alpha + \kappa\alpha^*) \sin(LD/2) - j\alpha D\cos(LD/2)}{D\cos(LD) + j\Delta \sin(LD)} \\ P_{31} &= -2P_{13} \\ P_{32} &= -2P_{23} \\ P_{33} &= -\frac{4}{D^3} \frac{[(\Delta^2 + |\kappa|^2)|\alpha|^2 + 2\Delta \text{Re}(\kappa^* \alpha^2)] [1 - \cos(LD)]}{D\cos(LD) + j\Delta \sin(LD)} + \\ & j \frac{4}{\Delta^2 - |\kappa|^2} \frac{[\Delta|\alpha|^2 + \text{Re}(\kappa^* \alpha^2)] \sin(LD)}{D\cos(LD) + j\Delta \sin(LD)} - j4L \frac{\Delta|\alpha|^2 + \text{Re}(\kappa^* \alpha^2)}{\Delta^2 - |\kappa|^2} + jL\omega C, \end{aligned} \quad (4)$$

where $D = \sqrt{\Delta^2 - |\kappa|^2}$, and L denotes the length of the device.

Furthermore, since practical SAW devices are typically composed of multiple transducers and reflection gratings, it is necessary to sequentially cascade each P -matrix unit to

calculate device response. Therefore, let P^A and P^B be the neighboring P -matrices cascaded from left to right; the cascading formula for the P -matrix is expressed as follows [10]:

$$\begin{aligned}
 P_{11} &= P_{11}^A + P_{11}^B \frac{P_{21}^A P_{12}^A}{1 - P_{11}^B P_{22}^A} \\
 P_{12} &= P_{21} = \frac{P_{12}^A P_{21}^B}{1 - P_{11}^B P_{22}^A} \\
 P_{22} &= P_{22}^B + P_{22}^A \frac{P_{12}^B P_{21}^B}{1 - P_{11}^B P_{22}^A} \\
 P_{13} &= P_{13}^A + P_{12}^A \frac{P_{13}^B + P_{11}^B P_{23}^A}{1 - P_{11}^B P_{22}^A} \\
 P_{23} &= P_{23}^B + P_{21}^B \frac{P_{23}^A + P_{22}^A P_{13}^B}{1 - P_{11}^B P_{22}^A} \\
 P_{33} &= P_{33}^A + P_{33}^B + P_{32}^A \frac{P_{13}^B + P_{11}^B P_{23}^A}{1 - P_{11}^B P_{22}^A} + P_{31}^B \frac{P_{23}^A + P_{22}^A P_{13}^B}{1 - P_{11}^B P_{22}^A}
 \end{aligned} \tag{5}$$

As for a single-port resonator without reflectors, P_{33} represents the admittance of the interdigital transducers (IDT). For this case, the boundary conditions are given by $a_1 = a_2 = 0$, and P_{33} represents the input admittance of the SAW resonator.

2.2. COM Parameter Extraction

A theoretical method to extract precise COM parameters based on FEM software COMSOL Multiphysics 5.5 is presented. Figure 2 shows the schematic of a quasi-three-dimensional periodic FEM model and a structure used for simulation. As shown, one period with periodic metal electrodes alternately applying a positive or negative voltage is considered, and a perfectly matched layer (PML) is applied to the bottom to reduce the model’s size and suppress the unwanted boundary reflection. Periodic boundary conditions were defined on the left (Γ_L) and right (Γ_R) of the model. In addition, the meshing grid elements in each domain of the model are applied, and the maximum size of the grid cells in each material is specified as one-sixteenth of the wavelength to accurately resolve the stress waves in the solid domain. Furthermore, each IDT requires at least three solid cells in the thickness direction to ensure the accuracy of the calculation. The details of the quasi-3D periodic FEM model are reported in our previous work [24]. The piezoelectric module involving the physical field of solid mechanic and electrostatic coupling with the temperature field is performed so that the temperature-dependent COM parameters can be obtained. For a given temperature (T), the thermal effect can be computed by incorporating the linear thermal expansion coefficients and temperature coefficients of elasticity into the model.

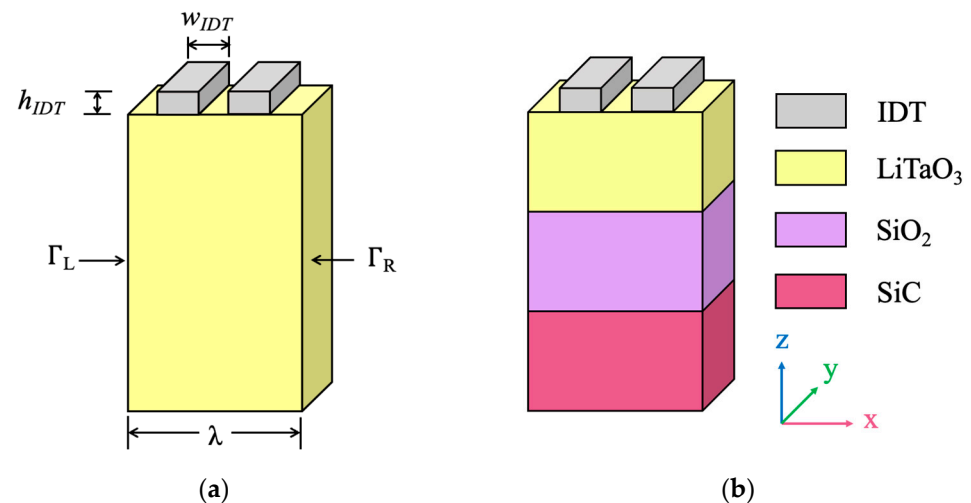


Figure 2. The schematic of the FEM model and structure used for simulation. (a) A SAW resonator on a 36°YX–LT substrate, and (b) a SAW resonator on a 36°YX–LT/SiO₂/SiC substrate.

Figure 3 shows the procedure for the extraction of COM parameters. As is shown, an eigen frequency and frequency domain analysis of the multiphysics quasi-3D periodic FEM model for the SAW resonator is performed. As shown, the symmetric frequency (f_{sc-}) and anti-symmetric frequency (f_{sc+}) can be obtained by performing eigen frequency analysis at short-circuited grating, and then the center frequency (f_0), v , and κ_p can be calculated using the following:

$$f_0 = \frac{f_{sc+} + f_{sc-}}{2}, \tag{6}$$

$$v = \lambda f_0, \tag{7}$$

$$\kappa_p = 2\pi \left(\frac{f_{sc-}}{f_0} - 1 \right). \tag{8}$$

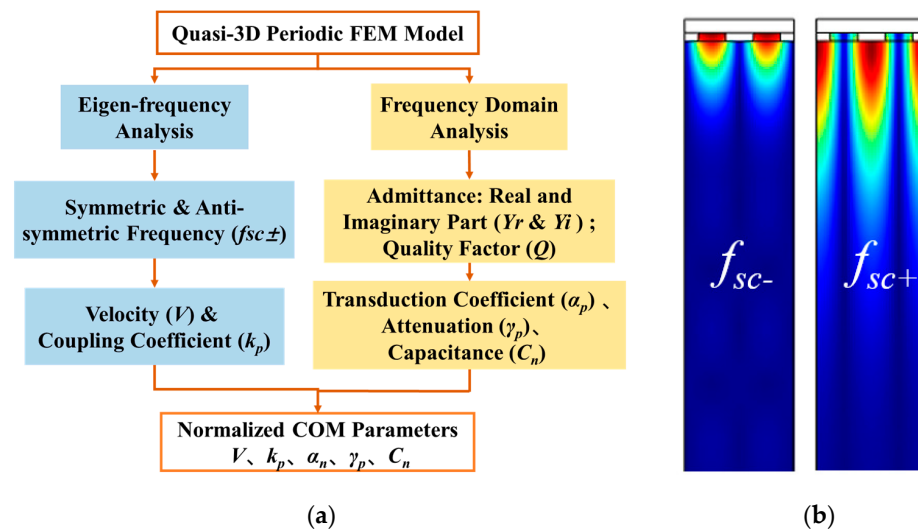


Figure 3. The FEM analysis with quasi-3D periodic structures: (a) the procedure of COM parameter extraction; (b) modal displacements at the stopband edges.

Frequency domain analysis of the proposed model allows for the determination of the admittance, Y , and Q factor of the SAW resonator, which can be calculated via harmonic analysis under the condition where a sinusoidal signal with voltage, $V/2$, is applied to the electrode. Then, the harmonic admittance, Y , per IDT period is estimated using $Y = 2\pi f j Q_c / V$, where f is the driving frequency and Q_c is the total charge induced on the electrode [24]. Therefore, the remaining COM parameters, α_p , γ_p , and C_p , can be obtained using the following formulas:

$$\alpha_p = \sqrt{\frac{Y_r \gamma_p}{4}}, \tag{9}$$

$$\gamma_p = \pi \frac{\Delta f}{f_0}, \tag{10}$$

$$C_p = \frac{2Y_r Q \left(\frac{f_{ar}}{f_{sc-}} - 1 \right)}{2\pi f_{ar} \left[4Q^2 \left(\frac{f_{ar}}{f_{sc-}} - 1 \right)^2 + 1 \right]}, \tag{11}$$

where Y_r is the conductance at the resonant frequency, Δf is the half-peak width of the conductance, f_{ar} is the anti-resonant frequency, and the quality factor is given by $Q = \frac{f_{sc-}}{\Delta f}$. When the above five COM parameters are available, the device response and temperature behavior of the SAW device can be calculated.

2.3. Model Verification

For validation, first, the COM parameters extracted using the proposed method are verified for the normal SAW resonator based on bulk $128^\circ\text{YX-LiNbO}_3$ substrate. Due to the almost negligible attenuation of Rayleigh waves excited on LiNbO_3 substrates, the attenuation coefficient was not extracted. Table 1 presents a comparison between the extracted COM parameters and those of the previously reported results taken from Refs. [25,26] in our previous work [27]. As can be seen, these extracted COM parameters at a temperature (T) of 25°C are compared well. Additionally, the COM parameters at a temperature (T) of 100°C are also calculated via the proposed method. It is obvious that the temperature-dependent COM parameters vary with the temperature change. Compared to the traditional COM and pure FEM methods, the proposed method takes into account the temperature effects, allowing for a combination of faster and more accurate consideration of practical influences when designing SAW devices in the manufacturing process. This enhances the alignment between the expected and achieved outcomes.

Table 1. COM parameters for $128^\circ\text{YX-LiNbO}_3$ with $h_{\text{IDT}} = 0$ [27].

Parameters	Ref. [25]	Ref. [26]	This Work	
T [$^\circ\text{C}$]	25	25	25	100
v [m/s]	3899.98	3901	3899	3876
κ_p [%]	-3.95	-3.95	-3.89	-3.93
α_n [$10^{-5} \Omega^{-\frac{1}{2}}$]	68.618	69.65	69.81	70.15
C_n [10^{-5} pF/ μm]	49.263	48.36	49.3	48.3

Then, the extracted COM parameters are employed to simulate the admittance of the SAW device with the P -matrix model. Figure 4 presents the calculated admittance of the multi-layered SH-SAW resonator on a $36^\circ\text{YX-LT/SiO}_2/\text{SiC}$ layered substrate. For comparison, the measurement taken from Ref. [28] is also presented. As shown, the admittance curves basically fit well, and there exists a small difference at the anti-frequency, which is mainly caused by a bulk wave. Nevertheless, it is noted that the proposed COM method accurately reproduces fluctuations at low frequencies and a spurious response at high frequencies.

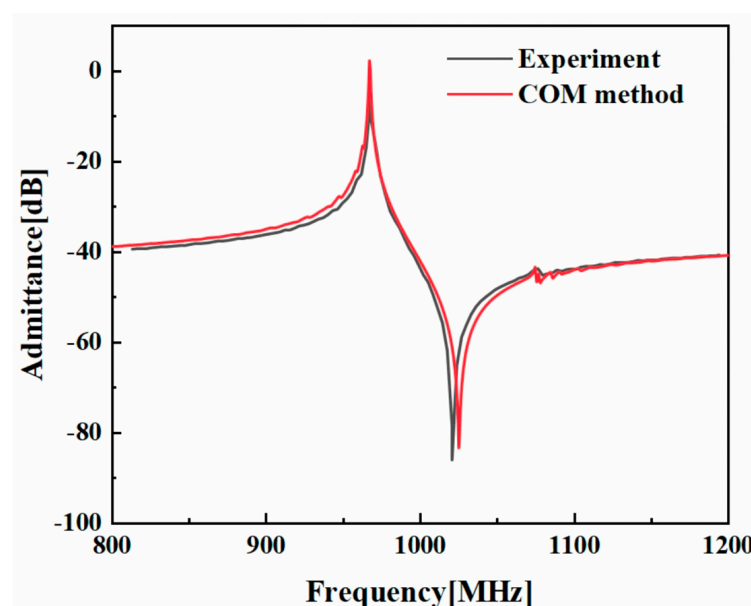


Figure 4. An admittance comparison between the proposed COM method and measured results [28] for the SAW resonator on a $36^\circ\text{YX-LT/SiO}_2/\text{SiC}$ multi-layered substrate.

3. Results and Discussion

3.1. Simulation of Resonators

Based on the advantages of fast and accurate simulations offered by the COM method, this work employs the COM method for the simulation and optimization of SAW resonators and DMS filters.

Figure 5 shows the calculated admittance of resonators for both bulk 36°YX-LT substrate and the $36^\circ\text{YX-LT/SiO}_2/\text{SiC}$ multi-layered structure. The structural parameters of the resonator are shown in Table 2. It can be observed that the multi-layered structure exhibits significantly higher K^2 and a larger oscillation amplitude. This can be attributed to the SiC substrate in the multi-layered structure, which has a higher velocity and thus offers an SAW energy confinement effect. This characteristic allows for the efficient conversion of electrical energy into mechanical vibration, enabling the high performance of SAW devices. Compared to the bulk LT substrate, the LT/SiO₂/SiC multi-layered substrate has advantages in terms of a higher Q and improved temperature stability. From this point on, the $36^\circ\text{YX-LT/SiO}_2/\text{SiC}$ multi-layered structure was further optimized in terms of different Euler angles and geometric structural parameters.

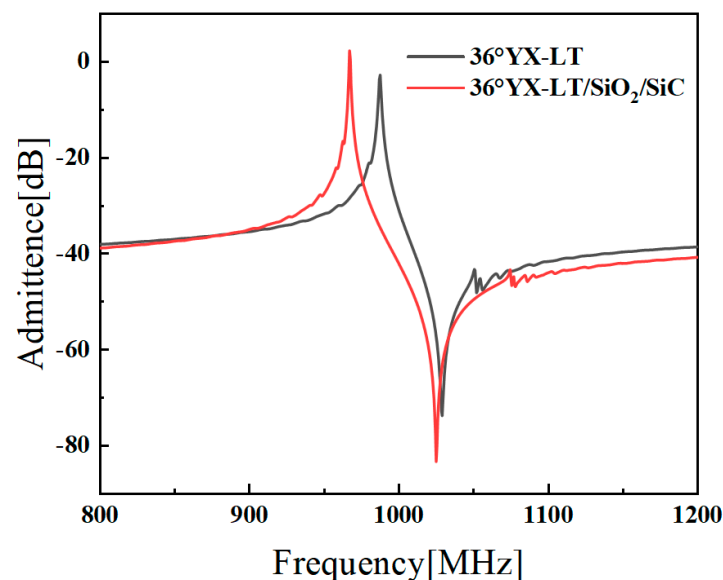


Figure 5. The admittance comparison between the SH-SAW resonator with bulk 36°YX-LT substrate and the SH-SAW resonator with the $36^\circ\text{YX-LT/SiO}_2/\text{SiC}$ multi-layered substrate.

Table 2. The geometric structure parameters of the SAW resonator.

Parameters	Value
Wavelength (λ)	4 (μm)
Aperture	15 * λ
IDT thickness	0.06 * λ
Metallization ratio	0.4
Number of IDT finger pairs	75
Number of reflector strips	40

The advantages of the multi-layered structure over those of a bulk LT structure, in terms of SAW resonator fabrication, typically result in a higher Q and improved temperature stability. Therefore, in this study, the multi-layered structure is optimized and employed for the simulation of SAW devices.

Figure 6a presents the calculated velocities and electromechanical coupling coefficients of an SH wave mode on the LT/SiO₂/SiC structure versus different β rotation angles of the LT layer. The maximum K^2 value of the device, which was approximately 13.88%, was

achieved by setting the Euler angle of the LT layer in the COMSOL as $(0^\circ, 151^\circ, 0^\circ)$ when the LT layer thickness at 800 nm. In this configuration, the phase velocity reached around 4064 m/s.

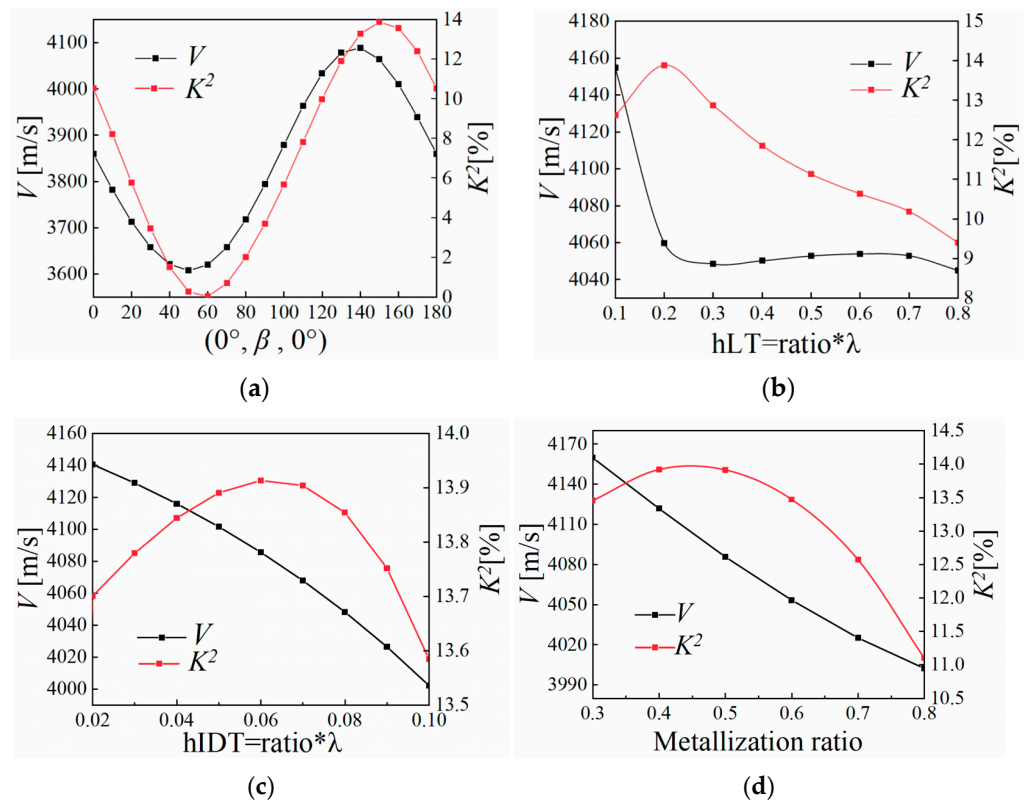


Figure 6. The calculated velocities and electromechanical coupling coefficients of the multi-layered structure versus the (a) β angles of the LT layer. The LT layer thickness is 800 nm. The metallization ratio is 0.5. The electrode thickness is 297 nm. (b) Piezoelectric layer thicknesses; $\beta = 151^\circ$. (c) Electrode thicknesses; $\beta = 151^\circ$. (d) Metallization ratios.

Additionally, Figure 6b illustrates the calculated velocities and electromechanical coupling coefficients versus different piezoelectric layer thicknesses on a $29^\circ\text{YX-LT/SiO}_2/\text{SiC}$ structure. A K^2 value of 13.89% is obtained when the piezoelectric layer thickness is 0.2 λ , with a corresponding phase velocity of 4060 m/s. This reduction in velocity is deemed acceptable compared to the case for a piezoelectric layer thickness of 0.1 λ . In the case of a 0.2 λ thick LT layer, a K^2 value of 13.91% is obtained when the electrode thickness is 0.06 λ , as shown in Figure 6c. It is worth noting that as the electrode thickness increases, the velocity of the SH wave mode gradually decreases due to the influence of mass loading. However, the velocity of 4085 m/s at the electrode thickness of 0.06 λ is an acceptable value. Under the condition of a 0.2 λ thick LT layer and 0.06 λ thick Al electrodes, an optimized structure with a maximum K^2 of 13.92% and suitable phase velocity of 4122 m/s obtained simultaneously results when the metallization ratio is 0.4.

Figure 7a presents the simulation results of the optimized resonator compared to those of a resonator on a 36°YX-LT substrate. The optimized resonator on the $29^\circ\text{YX-LT/SiO}_2/\text{SiC}$ structure exhibits significantly larger K^2 values and higher amplitudes compared to the resonator on a 36°YX-LT substrate. Figure 7b illustrates the temperature characteristics of the optimized resonator on the $29^\circ\text{YX-LT/SiO}_2/\text{SiC}$ structure. It is evident that as the temperature increases, the overall admittance gradually shifts to the left. The temperature coefficient of the resonance frequency (TCF_r) is $-10.67 \text{ ppm}/^\circ\text{C}$, while the temperature coefficient of the anti-resonance frequency (TCF_a) is $-40.36 \text{ ppm}/^\circ\text{C}$ [29–31]. Table 3 presents a comparison for the extracted COM parameters at different temperatures. As can be seen, these extracted temperature-dependent COM parameters vary with the temperature

change. The performance comparison between the resonators on a 36°YX-LT substrate and a $29^\circ\text{YX-LT/SiO}_2/\text{SiC}$ substrate is shown in Table 4. The multi-layered structure demonstrates a significant improvement in temperature stability, which effectively mitigates the impact of temperature variations on SAW resonators and meets the requirements for precise and stable performance in practical applications.

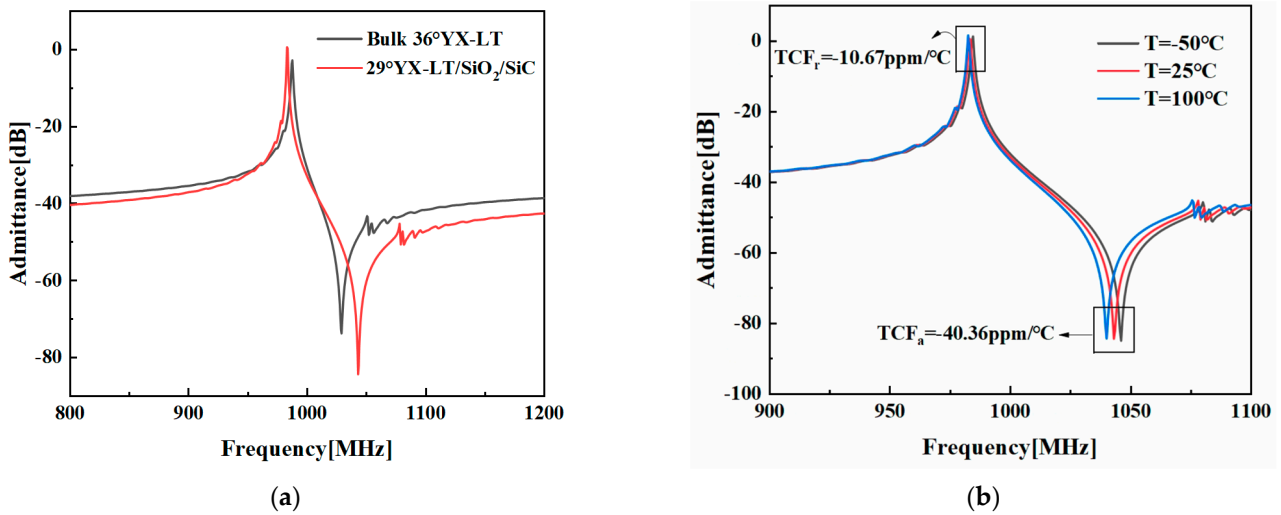


Figure 7. (a) The admittance comparison between the SH-SAW resonator on the 36°YX-LT substrate and the SH-SAW resonator on the optimized $29^\circ\text{YX-LT/SiO}_2/\text{SiC}$ structure. (b) Admittances of the optimized $29^\circ\text{YX-LT/SiO}_2/\text{SiC}$ structure at different temperatures.

Table 3. COM parameters for the $29^\circ\text{YX-LiTaO}_3$ structure.

Parameters	T = -50°C	T = 25°C	T = 100°C
v [m/s]	4128	4122	4116
κ_p [%]	-28.94	-28.66	-28.19
α_n [$10^{-5} \Omega^{-\frac{1}{2}}$]	86.93	86.62	85.83
C_n [$10^{-5} \text{pF}/\mu\text{m}$]	29.30	29.91	30.73
γ_p [/]	0.00231	0.00232	0.00232

Table 4. Performance comparison between the SAW resonators on the 36°YX-LT substrate and $29^\circ\text{YX-LT/SiO}_2/\text{SiC}$ substrate.

Structure Configuration	K^2 (%)	V (m/s)	TCF_r (ppm/ $^\circ\text{C}$)	TCF_a (ppm/ $^\circ\text{C}$)	Q_r
Bulk 36°YX-LT	10.16	4075	-30.21	-48.01	773
$29^\circ\text{YX-LT/SiO}_2/\text{SiC}$	13.92	4122	-10.67	-40.36	1265

3.2. Simulation of DMS Filters

The advantages of the optimized $29^\circ\text{YX-LT/SiO}_2/\text{SiC}$ structure over a 36°YX-LT structure typically imply a larger bandwidth and lower insertion loss for filters. Therefore, this work extends the optimization results of multi-layered SAW resonators and applies the optimized structure for a DMS filter simulation.

In order to obtain a wider bandwidth, the test DMS structure of three IDTs in which the lateral IDTs are symmetrically arranged with respect to the center IDT is used [32]. Figure 8 presents the electrode configuration. The corresponding parameters of DMS filters are shown in Table 5.

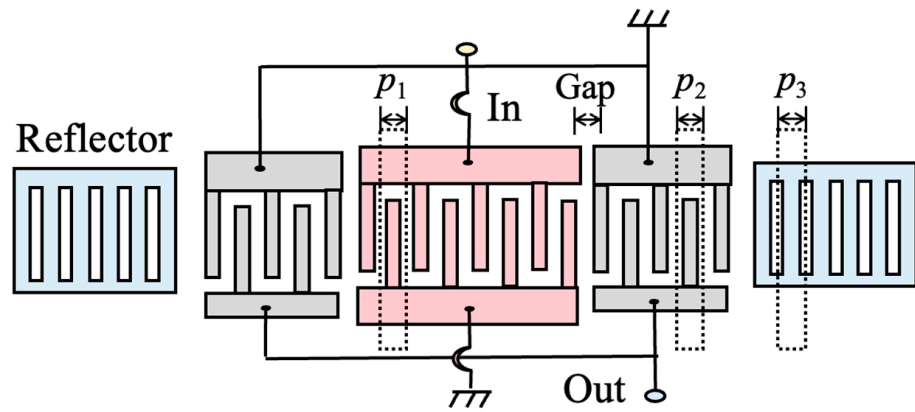


Figure 8. Configuration of a test DMS structure using the first mode and third mode.

Table 5. The geometric structure parameters of the DMS filter.

Parameters	Value
p_1	2 [μm]
p_2	1.9 [μm]
p_3	2.3 [μm]
Gap	1 [μm]
IDT finger pairs of the input part	15.5
IDT finger pairs of the output part	9
Number of reflector strips	60

Figure 9 illustrates a comparison of the transmission spectrums between the filters on the 36°YX-LT and $29^\circ\text{YX-LT/SiO}_2/\text{SiC}$ substrates. The DMS filter on the $29^\circ\text{YX-LT/SiO}_2/\text{SiC}$ substrate exhibits a significantly wider bandwidth compared to that of the common filter. This expanded bandwidth enables the filter to transmit a broader range of frequencies, meeting the requirements for processing various frequency signals. Additionally, the $29^\circ\text{YX-LT/SiO}_2/\text{SiC}$ structure demonstrates a flatter passband, ensuring uniform signal transmission and avoiding an uneven frequency response and distortion. This is crucial for applications that demand good signal quality and accuracy. Therefore, the DMS filter on the $29^\circ\text{YX-LT/SiO}_2/\text{SiC}$ substrate provides more flexible and high-performance signal processing capabilities.

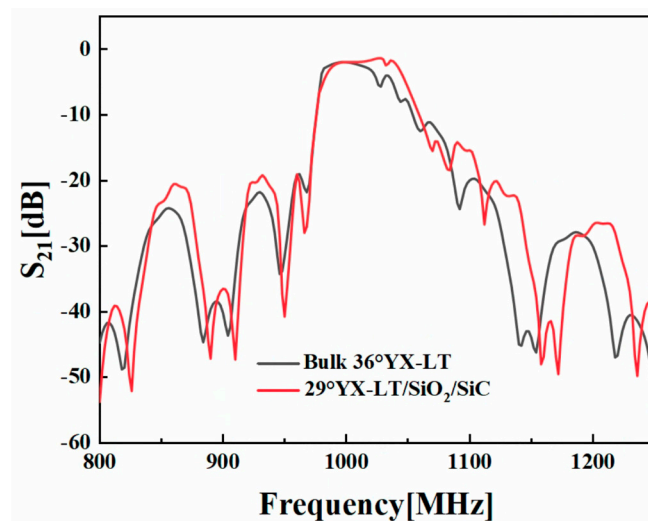


Figure 9. The transmission spectrum comparison between the DMS filters on the bulk 36°YX-LT substrate and the optimized $29^\circ\text{YX-LT/SiO}_2/\text{SiC}$ structure.

Figure 10 illustrates the computed temperature characteristics of the two DMS filters, indicating that the optimized $29^\circ\text{YX-LT/SiO}_2/\text{SiC}$ structure exhibits superior temperature stability compared to that of the 36°YX-LT structure. Particularly, TCF suppression is evident at lower frequencies in the $29^\circ\text{YX-LT/SiO}_2/\text{SiC}$ structure. TCF values at the lower edge (TCF_l) are reduced to $-14.35 \text{ ppm}/^\circ\text{C}$, while TCF values at the higher edge (TCF_h) are reduced to $-22.02 \text{ ppm}/^\circ\text{C}$ compared to those of the DMS filter on a 36°YX-LT structure ($\text{TCF}_l = -32.87 \text{ ppm}/^\circ\text{C}$, $\text{TCF}_h = -37.55 \text{ ppm}/^\circ\text{C}$). The $29^\circ\text{YX-LT/SiO}_2/\text{SiC}$ structure effectively suppresses the TCF to a satisfactory level, emphasizing its contribution to improved temperature stability. Table 6 presents the specific performance of the two DMS filters. In addition to the improvement in TCF, in-band insertion loss is optimized from -3 dB to -2 dB , effectively enhancing the application potential of the filter at high temperatures and enabling the better performance of signal transmission. It can be inferred that by employing the improved method, it is possible in the early stages of designing SAW devices to simulate the propagation characteristics and temperature properties of DMS filters rapidly and accurately in the manufacturing process. This facilitates the identification of filters that meet the expected requirements, enabling mass production and reducing material wastage caused by inaccurate or incomplete simulations.

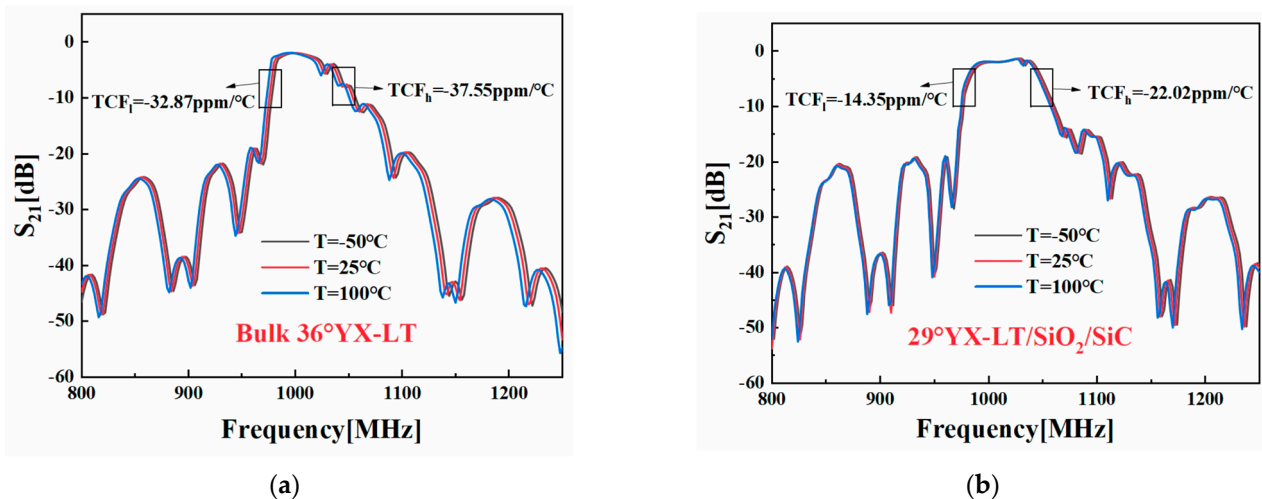


Figure 10. Simulated transmission spectra of DMS filters with (a) the bulk 36°YX-LT substrate and (b) the optimized $29^\circ\text{YX-LT/SiO}_2/\text{SiC}$ structure at different temperatures.

Table 6. Performance comparison between the two DMS filters based on a 36°YX-LT substrate and a $29^\circ\text{YX-LT/SiO}_2/\text{SiC}$ substrate.

Structure Configuration	Insert Loss (dB)	TCF_l ($\text{ppm}^\circ\text{C}^{-1}$)	TCF_h ($\text{ppm}^\circ\text{C}^{-1}$)
Bulk 36°YX-LT	-3	-32.87	-37.55
$29^\circ\text{YX-LT/SiO}_2/\text{SiC}$	-2	-14.35	-22.02

4. Conclusions

In this paper, an advanced method combining the COM theory with a quasi-3D periodic FEM model coupled with a thermal field is proposed. Accurate simulations and analyses of the electroacoustic and temperature behavior of SAW resonators and filters are performed. This is of great assistance in the manufacturing process of SAW devices, effectively preventing production wastage caused by inaccurate simulations or the neglect of temperature stability. On this basis, a comparison is made between resonators on a 36°YX-LT structure and those on a $29^\circ\text{YX-LT/SiO}_2/\text{SiC}$ multi-layered structure. This comparison demonstrates the advantages of the multi-layered structure with a larger K^2 of 13.92% and a lower TCF of $-10.67 \text{ ppm}/^\circ\text{C}$. Frequency response calculations are

performed for both the SAW resonators and filters based on this optimized structure, revealing significant improvements in performance compared to that of a normal structure. In particular, the temperature stability and the in-band insertion loss of the optimized DMS filter are improved, highlighting the tremendous potential of SAW filters in high-temperature applications.

Author Contributions: Conceptualization, Q.Z.; methodology, Q.Z. and Y.Y.; validation, L.L., B.L. and Q.Z.; writing—original draft preparation, L.L.; writing—review and editing, L.L., Q.Z. and Y.Y.; supervision, Q.Z., Y.T. and S.F.; project administration, X.Z.; funding acquisition, Q.Z. and Y.T. All authors have read and agreed to the published version of the manuscript.

Funding: This work is partially supported by Youth Science Fund of National Natural Science Foundation of China, grant number 12004413 and 11904233; the National Natural Science Foundation of China, grant number 12374449 and 52172005; Youth Innovation Promotion Association, Chinese Academy of Sciences (2022024) and the Research and Development Program in Significant Area of Guangzhou City, grant number 202206070001.

Data Availability Statement: Data are contained within the article.

Conflicts of Interest: The authors declare no conflict of interest.

References

1. Bartasyte, A.; Margueron, S.; Baron, T.; Oliveri, S.; Boulet, P. Toward High-Quality Epitaxial LiNbO₃ and LiTaO₃ Thin Films for Acoustic and Optical Applications. *Adv. Mater. Interfaces* **2017**, *4*, 1600998. [[CrossRef](#)]
2. Hashimoto, K.; Kadota, M.; Nakao, T.; Ueda, M.; Miura, M.; Nakamura, H.; Nakanishi, H.; Suzuki, K. Recent development of temperature compensated SAW Devices. In Proceedings of the 2011 IEEE International Ultrasonics Symposium, Orlando, FL, USA, 18–21 October 2011; pp. 79–86.
3. Shiba, T.; Ooki, M.; Hamasaki, J.; Hikino, O.; Fujita, Y. 6J-2 Study of High Isolation and Miniature SAW Duplexer. In Proceedings of the 2006 IEEE Ultrasonics Symposium, Vancouver, BC, Canada, 2–6 October 2006; pp. 1060–1064.
4. Takai, T.; Iwamoto, H.; Takamine, Y.; Fuyutsume, T.; Nakao, T.; Hiramoto, M.; Toi, T.; Koshino, M.I.H.P. SAW Technology and Its Application to Microacoustic Components (Invited). In Proceedings of the 2017 IEEE International Ultrasonics Symposium (IUS), Washington, DC, USA, 6–9 September 2017.
5. Li, Q.; Fu, S.-L.; Song, C.; Wang, G.-Y.; Zeng, F.; Pan, F. Improved resistance to electromigration and acoustomigration of Al interdigital transducers by Ni underlayer. *Rare Met.* **2018**, *37*, 823–830. [[CrossRef](#)]
6. Urabe, S.; Uno, T.; Onuki, K. SAW Device Application to Public Telecommunication System in Japan. *Jpn. J. Appl. Phys.* **1983**, *22*, 12. [[CrossRef](#)]
7. Fujimaki, T.; Suzuki, M.; Kakio, S. Analysis of leaky surface acoustic waves on LiNbO₃ or LiTaO₃ thin plate bonded to similar-material substrates. *Jpn. J. Appl. Phys.* **2020**, *59*, SKKC01. [[CrossRef](#)]
8. Naumenko, N.F. High-velocity non-attenuated acoustic waves in LiTaO₃/quartz layered substrates for high frequency resonators. *Ultrasonics* **2019**, *95*, 1–5. [[CrossRef](#)] [[PubMed](#)]
9. Su, R.; Fu, S.; Shen, J.; Lu, Z.; Xu, H.; Wang, R.; Song, C.; Zeng, F.; Wang, W.; Pan, F. Wideband Surface Acoustic Wave Filter at 3.7 GHz With Spurious Mode Mitigation. *IEEE Trans. Microwave Theory Techn.* **2023**, *71*, 480–487. [[CrossRef](#)]
10. Plessky, V.; Koskela, J. Coupling-of-Modes Analysis of Saw Devices. *Int. J. High Speed Electron. Syst.* **2000**, *10*, 867–947. [[CrossRef](#)]
11. Kazuhiro Hirota, K.H.; Kiyoshi Nakamura, K.N. Equivalent Circuit of Interdigital Transducers Based on Coupling-of-Modes Theory Considering Electrode Resistivity and Propagation Loss. *Jpn. J. Appl. Phys.* **1994**, *33*, 2972. [[CrossRef](#)]
12. Huang, Y.; Bao, J.; Li, X.; Zhang, B.; Omori, T.; Hashimoto, K. Parameter extraction of coupling-of-modes equations including coupling between two surface acoustic waves on SiO₂/Cu/LiNbO₃ structures. *Jpn. J. Appl. Phys.* **2018**, *57*, 07LD13. [[CrossRef](#)]
13. Tang, G.; Goto, R.; Nakamura, H. Modeling and Suppression Method for Guided Mode in TC-SAW Devices. In Proceedings of the 2019 IEEE International Ultrasonics Symposium (IUS), Glasgow, UK, 6–9 October 2019; pp. 2087–2090.
14. Koshiba, M.; Ohbuchi, K. An Analysis of Surface-Acoustic-Wave Devices Using Coupling-of-Mode Theory and Finite-Element Method. *Jpn. J. Appl. Phys.* **1991**, *30*, 140. [[CrossRef](#)]
15. Shaposhnikov, K.; Kaltenbacher, M.; Nicolay, P. Fast full-FEM computation of COM parameters. Application to multilayered SAW structures. In Proceedings of the 2014 IEEE International Ultrasonics Symposium, Chicago, IL, USA, 3–6 September 2014; pp. 1501–1504.
16. Laude, V.; Reinhardt, A.; Ballandras, S.; Khelif, A. Fast FEM/BEM computation of SAW harmonic admittance and slowness curves. In Proceedings of the IEEE Ultrasonics Symposium, Montreal, QC, Canada, 23–27 August 2004; Volume 1, pp. 445–448.
17. Dufilie, P.; Ventura, P.; Hecht, F. COM parameters for thick metal and partially buried electrodes extracted from a mixed FEM/BEM numerical model. In Proceedings of the 2012 IEEE International Ultrasonics Symposium, Dresden, Germany, 7–10 October 2012; pp. 807–810.

18. Ventura, P.; Hode, J.M.; Solal, M.; Desbois, J.; Ribbe, J. Numerical methods for SAW propagation characterization. In Proceedings of the 1998 IEEE Ultrasonics Symposium, Sendai, Japan, 5–8 October 1998; Volume 1, pp. 175–186.
19. Solal, M.; Chen, L.; Gratier, J. Measurement and FEM/BEM simulation of transverse effects in SAW resonators in lithium tantalate. In Proceedings of the 2010 IEEE International Ultrasonics Symposium, San Diego, CA, USA, 11–14 October 2010; pp. 175–180.
20. Laude, V.; Reinhardt, A.; Wilm, M.; Khelif, A.; Ballandras, S. Fast FEM/BEM Simulation of SAW Devices via Asymptotic Waveform Evaluation. *IEEE Trans. Ultrason. Ferroelectr. Freq. Control* **2004**, *51*, 359–363. [[CrossRef](#)] [[PubMed](#)]
21. Taziev, R.M. FEM/BEM for Simulation of LSAW Devices. *IEEE Trans. Ultrason. Ferroelectr. Freq. Control* **2007**, *54*, 2060–2069. [[CrossRef](#)] [[PubMed](#)]
22. Plessky, V.P. A two parameter coupling-of-modes model for shear horizontal type SAW propagation in periodic gratings. In Proceedings of the 1993 Proceedings IEEE Ultrasonics Symposium, Baltimore, MD, USA, 31 October–3 November 1993; Volume 1, pp. 195–200.
23. Abbott, B.P.; Hashimoto, K. A coupling-of-modes formalism for surface transverse wave devices. In Proceedings of the 1995 IEEE Ultrasonics Symposium. Proceedings. An International Symposium, Seattle, WA, USA, 7–10 November 1995; Volume 1, pp. 239–245.
24. Zhang, Q.; Han, T.; Chen, J.; Wang, W.; Hashimoto, K. Enhanced coupling factor of surface acoustic wave devices employing ScAlN/diamond layered structure with embedded electrodes. *Diam. Relat. Mater.* **2015**, *58*, 31–34. [[CrossRef](#)]
25. Lin, J. Precise and full extraction of the coupling-of-mode parameters with periodic Green's function. *Sci. China Ser. F* **2003**, *46*, 298. [[CrossRef](#)]
26. Sun, X.; Zhou, S.; Cheng, J.; Lin, D.; Liu, W. Full extraction of the COM parameters for Rayleigh type surface acoustic wave. *AIP Adv.* **2022**, *12*, 025007. [[CrossRef](#)]
27. Li, L.; Zhang, Q.; Li, B.; Tian, Y.; Li, H. A New Method for Temperature Dependent COM Parameters Extraction and Its Application to Simulation of SAW Devices. In Proceedings of the International Congress on Ultrasonics, Beijing, China, 18–21 September 2023.
28. Wu, Z.; Wu, S.; Qian, H.; Bao, F.; Yang, G.; Zou, J.; Tang, G. High-Q SH-SAW Resonator Using 36° YX–LiTaO₃ on SiC. In Proceedings of the 2022 Joint Conference of the European Frequency and Time Forum and IEEE International Frequency Control Symposium (EFTF/IFCS), Paris, France, 24–28 April 2022; pp. 1–4.
29. Shen, J.; Fu, S.; Su, R.; Xu, H.; Lu, Z.; Zhang, Q.; Zeng, F.; Song, C.; Wang, W.; Pan, F. SAW Filters With Excellent Temperature Stability and High Power Handling Using LiTaO₃/SiC Bonded Wafers. *J. Microelectromech. Syst.* **2022**, *31*, 186–193. [[CrossRef](#)]
30. Tohyama, K.; Hori, Y.; Iwasaki, Y.; Suzuki, K. A Study on Temperature-Compensated Hybrid Substrates for Surface Acoustic Wave Filters. In Proceedings of the 2010 IEEE International Ultrasonics Symposium, San Diego, CA, USA, 11–14 October 2010.
31. Lu, Z.; Fu, S.; Chen, Z.; Shen, J.; Su, R.; Wang, R.; Song, C.; Zeng, F.; Wang, W.; Pan, F. High-frequency and high-temperature stable surface acoustic wave devices on ZnO/SiO₂/SiC structure. *J. Phys. D Appl. Phys.* **2020**, *53*, 305102. [[CrossRef](#)]
32. Morita, T.; Watanabe, Y.; Tanaka, M.; Nakazawa, Y. Wideband low loss double mode SAW filters. In Proceedings of the IEEE 1992 Ultrasonics Symposium Proceedings, Tucson, AZ, USA, 20–23 October 1992; pp. 95–104.

Disclaimer/Publisher's Note: The statements, opinions and data contained in all publications are solely those of the individual author(s) and contributor(s) and not of MDPI and/or the editor(s). MDPI and/or the editor(s) disclaim responsibility for any injury to people or property resulting from any ideas, methods, instructions or products referred to in the content.